High-Performance, Superparamagnetic, Nanoparticle-Based Heavy Metal Sorbents for Removal of Contaminants from Natural Waters

Cynthia L. Warner,[a] R. Shane Addleman,[a] Anthony D. Cinson,[a] Timothy C. Droubay,[a] Mark H. Engelhard,[a] Michael A. Nash,[b] Wassana Yantasee,[c] and Marvin G. Warner*[a]

We describe the synthesis and characterization of high-performance, superparamagnetic, iron oxide nanoparticle-based, heavy metal sorbents, which demonstrate excellent affinity for the separation of heavy metals in contaminated water systems (i.e., spiked Columbia River water). The magnetic nanoparticle sorbents were prepared from an easy-to-synthesize iron oxide precursor, followed by a simple, one-step ligand exchange reaction to introduce an affinity ligand to the nanoparticle surface that is specific to a heavy metal or class of heavy metal contaminants. The engineered magnetic nanoparticle sorbents have inherently high active surface areas, allowing for increased binding capacities. To demonstrate the performance of the nanoparticle sorbents, river water was spiked with specific metals and exposed to low concentrations of the functionalized nanoparticles. In almost all cases, the nanoparticles were found to be superior to commercially available sorbent materials as well as the unfunctionalized iron oxide nanoparticles.

Introduction

Remediation of aqueous systems contaminated with heavy metals is receiving increased attention as more information on their toxic effects to humans and the environment becomes known. In addition, increased population growth is placing pressure on water resources and widespread global industrialization is releasing large amount of pollutants contaminating more of the world's water supplies.[1,2] Ceramic metal oxides are traditionally used for the remediation of heavy metals, but these materials bind non-specifically and reversibly and can easily become saturated with ubiquitous species, such as Ca, Mg, and Zn.[2] In addition, separation and recovery of these sorbent materials from the decontaminated water can be extremely challenging. To overcome some of these issues, attention has been focused on magnetic sorbent materials for the capture and removal of toxic species. We have recently shown the efficacy of functionalized iron oxide nanoparticles as both sorbents for a number of toxic heavy metal contaminants in aqueous systems,[3] as well as the sensing element for electrochemical detection of heavy metals in complex sample matrices, for example, contaminated waters and biological fluids.[4] These studies have produced very promising results regarding the potential use of nontoxic, relatively inexpensive, surface-tailored, magnetic iron oxide nanoparticles in environmental applications, such as remediation and sensing.[4–19]

Superparamagnetic, iron oxide nanoparticle-based materials have been demonstrated to be excellent heavy metal sorbents owing in part to their high surface area per mass ($>$ 100 $m^2 g^{-1}$), their superparamagnetic properties that prevent magnetic agglomeration when dispersed, and that they can be easily removed from a sample system by applying an external magnetic field. The addition of small molecule affinity ligands to the surface of the nanoparticles has also been shown to greatly increase the sorbent's affinity for specific heavy metals, however, imparting this functionality can be synthetically challenging and difficult to scale up. Despite these challenges, solid-phase extraction of heavy metals using magnetic nanoparticles has been demonstrated by a number of groups[5] who have shown the removal of a specific heavy metal contaminant using polymer encased and surface functionalized magnetic nanoparticles,[3,6–14] as well as bare iron oxide nanoparticles (both magnetite and maghemite).[15–18] In the majority of cases reported in the literature, the synthetic methods used to produce the nanoparticles provide materials with an affinity toward either a single analyte or a narrow class of analytes. One of the primary advantages of the approach reported here is that the magnetic nanoparticle sorbent materials all contain an organic ligand (Scheme 1), with a demonstrated affinity for binding toxic heavy metals that can easily be changed to alter the reactivity of the resultant nanoparticles. The specific ligands reported here were chosen to provide a route to tune the affinity and heavy metal specificity of this novel class of nanoparticle-based heavy metal sorbents.

[a] C. L. Warner, Dr. R. S. Addleman, A. D. Cinson, Dr. T. C. Droubay, Dr. M. H. Engelhard, Dr. M. G. Warner
Pacific Northwest National Laboratory, Richland, WA 99352 (USA)
Fax: (+1) (509) 372-4583,
E-mail: marvin.warner@pnl.gov

[b] M. A. Nash
Department of Bioengineering, University of Washington
Seattle, WA 98195 (USA)

[c] Dr. W. Yantasee
Department of Biomedical Engineering, Oregon Health Sciences University
Portland, OR 97239 (USA)

WILEY InterScience®
DISCOVER SOMETHING GREAT

These are not the final page numbers! ↗↗
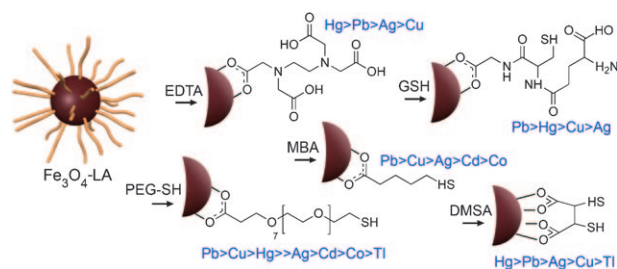
Scheme 1. Ligand exchange reaction of lauric acid-modified iron oxide nanoparticles (Fe_3O_4-LA) with the indicated ligands yield the functionalized magnetic nanoparticle sorbents with high affinity for the heavy metals indicated in blue. Ligand attachment to the nanoparticle is for illustrative purposes only and is not meant to suggest specific binding orientation or ligand conformation on the nanoparticle surface. The ligand abbreviations are as follows: LA, lauric acid; EDTA, ethylenediamine tetraacetic acid; GSH, L-glutathione; MBA, mercaptobutyric acid; PEG-SH, α-thio-ω-(propionic acid) hepta(ethylene glycol); DMSA, *meso*-2,3-dimercaptosuccinic acid.

Another benefit of this method is the use of a common precursor to produce nanoparticles with a wide range of functionality on the surface. Preparation of the iron oxide core was performed via high-temperature decomposition[20] to generate a monodisperse, superparamagnetic, iron oxide nanoparticle passivated with an organic soluble surfactant, in this case, lauric acid (LA). Nanoparticles prepared using this method are of higher purity (less trace metal contaminants), are highly crystalline, and are superparamagnetic with high saturation magnetization at room temperature with no remnant coercivity. In addition, the small size of the LA-stabilized nanoparticles (ca. 8 nm in diameter) imparts a very high active surface area ($> 100\ m^2 g^{-1}$) to the nanoparticles. These properties make the nanoparticles ideal sorbent candidates for application to a wide range of separation and sensing challenges, including both batch capture experiments like those reported here, as well as large volume separations that would be performed under flow conditions. The hydrophilic magnetic nanoparticle sorbents were produced from the precursor nanoparticle via a flexible ligand exchange reaction that allowed for the incorporation of a wide range of functional groups into the nanoparticle's ligand shell without altering the desirable properties of the precursor nanoparticle.

Although a variety of acid, silane, and diol head groups[21–26] have been shown to have an interaction with the iron oxide surface, the ubiquitous nature of the carboxylate containing ligand made it the most useful anchor group for generating a wide range of magnetic nanoparticle sorbents that contain functional groups of interest (thiol, amine, polyethylene glycol (PEG), and carboxylate (COO—)) at the periphery of the ligand shell. Since the carboxylate-containing ligands are only weakly bound to the surface, carboxylate-for-carboxylate ligand exchange can be performed using a variety of exchange conditions,[27,28] although the rate largely depends on the structure of the incoming ligand and the solvent system used. All of the magnetic nanoparticle sorbents described in this paper were prepared using the same solvent system and exchange conditions, which encouraged miscibility of both the hydrophobic nanoparticle precursor and the water-soluble ligand, promot-

ing successful exchange without the need for a phase-transfer catalyst or the decreased kinetics of a biphasic exchange process.[29]

Whereas there are many possible applications of the nanomaterials reported here, we chose, for this particular study, to describe their efficacy as heavy metal sorbents that might one day help to solve the global drinking water contamination problem. All of the extraction data presented in this effort was collected from real-world aqueous environmental samples taken from the Columbia River in eastern Washington State. The synthetic and characterization methods presented here allow fine-tuning of the surface chemistry of the nanoparticles to dramatically influence their chemical specificity and affinity. In addition, these methods offer a facile way to influence the materials' dispersibility and stability, which is essential for environmental applications focused on heavy metal remediation and decontamination.

Results and Discussion

Selection of magnetic nanoparticle sorbent ligand structures

The ligands employed in this work (Scheme 1) were selected owing to their demonstrated performance as chelators of toxic heavy metal, although the utility of many of the materials extend beyond the realm of environmental remediation into clinical application such as heavy metal decorporation from the human body. In addition, none of the described ligands, need to be synthesized as all can be purchased in their usable form. As an example, we have shown that iron oxide nanoparticles stabilized with *meso*-2,3-dimercaptosuccinic acid (DMSA) make excellent sorbents for toxic heavy metals in a variety of media,[3,4] but literature exists describing antibody conjugation to these same nanoparticles for use in biological systems for separation and detection.[30] Because the orientation of the thiol affinity moiety on the nanoparticle surface can have a significant effect on the binding potential towards a specific heavy metal ion,[31] the use of a variety of thiol-containing ligands allowed us to explore which ligands allowed for maximal analyte binding. The mono-thiol containing 4-mercaptobutyric acid (MBA), as well as the biologically relevant, thiol-containing, tripeptide glutathione (GSH) and thiol-modified α-thio-ω-(propionic acid) hepta(ethylene glycol) (PEG-SH) ligands were used. The prepared nanoparticles containing the described thiol functionalities are easily dispersed in water. Finally, ethylenediamine tetraacetic acid (EDTA) was an obvious ligand choice since it is a well-known chelator of toxic metals[32] in chelation therapies in the body and environment, however, it has the disadvantage that removal of the metal–EDTA species following treatment is still a challenge in the environment.[33] EDTA bound to a magnetic particle enables removal of the metal–EDTA complex through the application of a relatively low-strength magnetic field, a more direct process for the treatment of natural waters and clinical samples, including blood and urine.

↖↖ These are not the final page numbers!

Physical characteristics of exchanged Fe_3O_4 nanoparticles

The magnetic nanoparticle sorbent materials were fully characterized before and following ligand exchange to ensure retention of size, magnetic character, and successful surface coverage with the functional hydrophilic ligand. Each magnetic nanoparticle sorbent was then dispersed in a solution of river water spiked with seven of the most environmentally significant heavy metals, Hg, Pb, Cd, Ag, Co, Cu, and Tl, to determine its affinity for each metal. Since all of the hydrophilic affinity ligands chosen are multidentate or contain functional groups vulnerable to oxidation, for example thiols, ligand-induced aggregation was a concern when dispersed in contaminated media. Analysis of the materials using a variety of techniques confirmed this behavior, although the occurrence appeared to have minimal impact on the performance of the materials as heavy metal sorbents; this is discussed below in detail. The results of the characterization of the materials (see Experimental Section) are summarized in Table 1 and discussed below in more detail. In general, it is important to note that the method reported here to chemically functionalize the surface does not adversely impact the physical properties (namely size, aqueous dispersibility, and magnetic susceptibility) of the starting LA-nanoparticles.

Brennaur-Emmet-Teller (BET) analysis was used to measure the specific surface area of the modified and bare Fe_3O_4 nanoparticles. The results showed, that in each case the measured surface area of the nanoparticles is similar before and after ligand exchange, typically >100 $m^2 g^{-1}$. BET results for Fe_3O_4-LA failed to produce usable data, which could be attributed to the fatty acid layer promoting the formation of a semi-solid/waxy-phase when cooled for the assay with no measureable data owing to solidification of the particles. Theoretical surface calculations based on a face-centered cubic (fcc) hard sphere model using the nanoparticle core diameters measured by TEM give a value similar to that measured for the water-soluble ligand-stabilized nanoparticles. Both theoretical and measured specific surface area values are reported in Table 1 for each modified nanoparticle core; each measured value is in agreement with the calculated theoretical value. The measured

surface area of ca. 86 $m^2 g^{-1}$ for the PEG-SH-modified nanoparticles was slightly lower than expected; the long PEG chain likely prevents close packing of the ligand when binding through the acid head group and could potentially render the partially passivated surface more vulnerable to agglomeration.

TEM analysis confirmed the retention of particle size following exchange for a hydrophilic ligand (Figure 1). The precursor nanoparticle has a core diameter of ca. 8.2 ± 2 nm and the
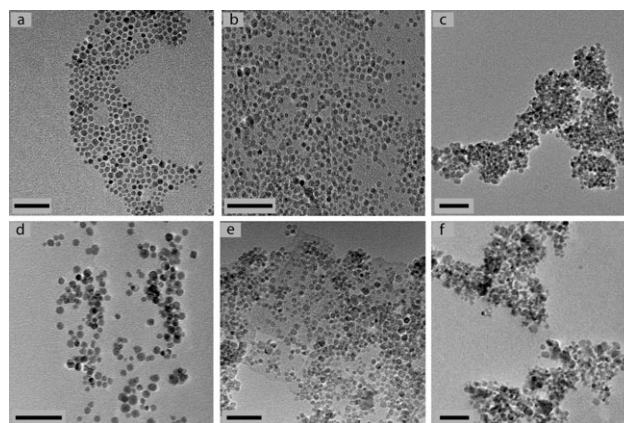

Figure 1. TEM images of precursor and water-soluble sorbent materials following ligand exchange: (a) Fe_3O_4-LA, (b) Fe_3O_4-DMSA, (c) Fe_3O_4-MBA, (d) Fe_3O_4-PEG-SH, (e) Fe_3O_4-GSH, and (f) Fe_3O_4-EDTA. Scale bar in each image denotes 20 nm.

water-soluble materials range from ca. 7.1–8.2 nm following exchange. The images of nanoparticles containing hydrophilic ligands exhibit varying degrees of ligand-induced aggregation; this behavior is expected and BET analysis confirms that the core size itself is not affected. Preservation of the small core size maintains the superparamagnetic character of the nanoparticle, which is a size dependent physical property and depends on the presence of discreet nanoparticles with a diameter of less than ca. 20 nm.[34] Thermal gravimetric analysis (TGA) of the functionalized materials (Figure 2) provides a rough estimate of the number of ligands present per nanoparticle. The percentage of material lost over the entire temperature range was used with the average nanoparticle diameter from TEM to calculate how many ligands are present per particle. That value is then compared with the theoretical expected value based on a carboxylate footprint of 0.34 nm^2, shown in Table 1.[35] It would be expected that the single-chain carboxylate-containing ligands would exhibit the closest packing behavior and this was indeed confirmed for the MBA and LA-modified materials. The presence of excess or-

Table 1. Physical properties of functionalized Fe_3O_4 nanoparticles.

Functionalized nano-particles	Surface area [$m^2 g^{-1}$]		Size [nm]	Magnetic susceptibility M_s [emu g^{-1}]	TGA [% mass loss]	# of ligands per particle	
	measured	theoretical[a]				calculated from TGA	theoretical[b]
Fe_3O_4-LA	–	103.1	8.3 ± 2	50.0	24.8	1158	768
Fe_3O_4-MBA	108.0	107.5	7.9 ± 1.2	59.8	12.1	813	575
Fe_3O_4-GSH	111.6	111.2	7.7 ± 1.3	47.4	16.4	398	548
Fe_3O_4-PEG-SH	86.33	104.1	8.2 ± 1.4	62.5	15.3	301	621
Fe_3O_4-DMSA	114	119.1	7.2 ± 2	53.8	7.7	258	478
Fe_3O_4-EDTA	106.8	103.9	8.2 ± 1.3	66.0	10.0	242	621

[a] Theoretical surface area was calculated using a fcc hard sphere model based on nanoparticle diameters obtained from TEM analysis. Upper and lower ranges represent the standard deviation obtained from the TEM size analysis. [b] The theoretical number of ligands per nanoparticle was calculated using the average core diameter from TEM and a carboxylate footprint of 0.34 nm^2 and assuming defect free monolayer coverage.[35]

These are not the final page numbers! ↗↗
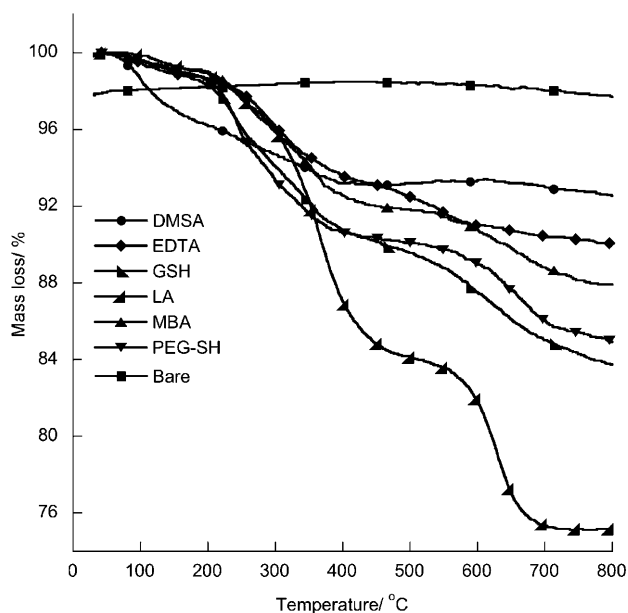
Figure 2. TGA curves for the bare, LA, and hydrophilic affinity ligand-modified Fe_3O_4 nanoparticles.

ganic material over what was expected for the LA ligand shell, is corroborated by the presence of the two-staged mass loss peaks by TGA suggesting interdigitation of the ligands, an observation described in previously reported TGA results for LA,[36] phosphonic acid,[25] and oleic acid-stabilized nanoparticles.[37,38] We suspect that the MBA-modified particles show a much higher ligand loading owing to the formation of disulfide bonds from the oxidation of the free thiols. The ramification of disulfide formation with this ligand on extraction efficiency is described below in more detail. The packing of the bulkier ligands that contain multiple carboxylate moieties should be less than expected from theoretical calculations when compared to monodentate ligands, for example MBA, a characteristic observed for the GSH, EDTA, PEG-SH, and DMSA-modified nanoparticles. The PEG-SH-modified particles exhibit the lowest ligand density, suggesting some disorder within the ligand film, and possibly attributed to the potential for the ether oxygens within the ligand to interact with the iron oxide surface leading to wrapping of the ligand across the surface rather than close packed binding through the acid head group.

FTIR spectroscopy was used to confirm adsorption of the water-soluble ligand to the iron oxide surface. Analysis of the nanoparticles before and after exchange showed the characteristic Fe—O absorption bands at ca. 580 cm^{-1} and 630 cm^{-1}. Binding of the ligand to the iron oxide surface through the carboxylate anion is evidenced by the COO$^-$ bands at ca. 1600 cm^{-1} ($v_a(CO_2^-)$) and 1400 cm^{-1} ($v_s(CO_2^-)$).[39] The exact position of these bands vary for the materials with different functionalities, seemingly owing to differences in the degree of surface coverage and packing density of the various ligands. It would be expected that the thiol-modified particles would have a small S—H stretching band near 2550 cm^{-1}, but this is typically weak and often unobserved in thin films such as the

nanoparticle ligand shell.[39] This absorption peak was not observed in the spectra for any of the thiol-modified materials, thus other absorption bands were identified for IR characterization. Specifically, this complicated the identification of the DMSA and MBA-modified materials by FTIR and required comparison of LA-modified particle features to subtle changes observed in the water-soluble ligand-modified particles. The LA nanoparticles display C—H stretching vibrations at 2850 cm^{-1} and 2920 cm^{-1} (methylene symmetric and asymmetric, respectively), and symmetrical methyl C—H stretches at 2958 cm^{-1}. The clear decreased intensity or complete disappearance of these bands was used to monitor the exchange of surface ligands for DMSA and MBA functionalized nanoparticles. The PEG—SH functionalized nanoparticle contains an ethylene glycol asymmetric stretching band at 1104 cm^{-1}. The spectrum for the GSH nanoparticles shows a N—H stretching band at 3411 cm^{-1}, as well as the N—H amide II bend at ca. 1550 cm^{-1}. The EDTA functionalized nanoparticles exhibit a small C—N stretching band at 1020 cm^{-1} and an O—H band at 3430 cm^{-1}.

X-ray photoelectron spectroscopy (XPS) analysis of the magnetic nanoparticle sorbents shows features consistent with organic ligands binding through the carboxylate anion to the iron oxide core (Figure 3). The carbon 1s spectrum for all of the materials show a peak at 284.8 eV characteristic of C—H and C—C bonds of a hydrocarbon chain, as well as a peak at ca. 288.5 eV indicative of carbon in a carboxylic acid environment.[40] The PEG-SH-modified particles also show a peak at ca. 286.5 eV for the C—O bonds from the PEG groups within the ligand. The four sorbent nanoparticles that contain thiol functional groups display a S 2p peak at 163.5 eV, a band position consistent with free thiols.[41,42] The intensity of this peak
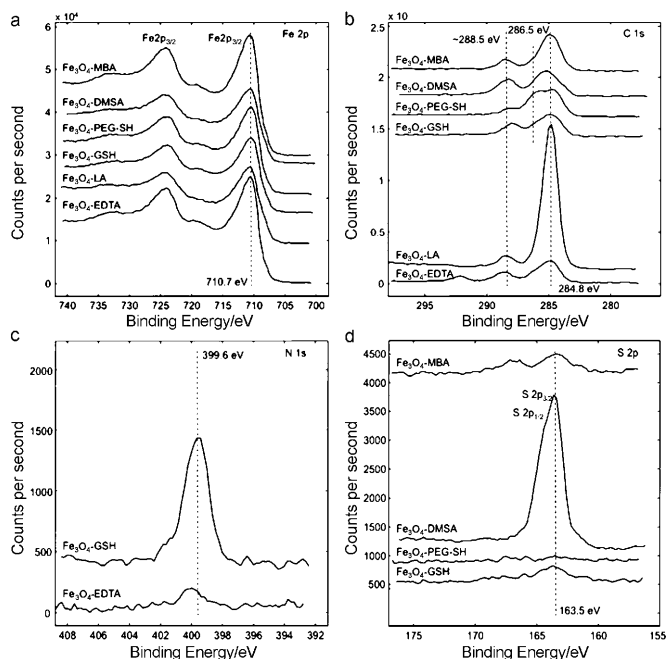

Figure 3. XPS spectra of functionalized magnetic nanoparticle sorbents: (a) Fe 2p peaks, (b) C 1s peak for each nanoparticle, (c) N containing species N 1s peak, and (d) thiol-containing species represented in the S 2p peak.

↖↖ These are not the final page numbers!

is the greatest for Fe_3O_4-DMSA with its di-thiol structure, followed by 4-mercaptobutyric acid, glutathione, and the barely detected S2p for the PEG-SH nanoparticles (see the Supporting Information for intensity values). The small intensity of the PEG-SH S2p peak could be attributed to the decreased packing density owing to steric crowding of the long PEG chains on the surface of the magnetic nanoparticle. The very small peak at ca. 167 eV associated with the MBA sample is likely attributed to an oxidized sulfur species contaminant but was not further identified and characterized. The N1s peaks are shown for glutathione and EDTA at 399.6 eV; the peak intensity for glutathione is much greater than that for EDTA suggesting a higher surface coverage of glutathione compared to EDTA, a fact supported by the measured TGA data. The $Fe\,2p_{3/2}$ peak located at 710.7 eV is consistent with that reported for magnetite, but the presence of a very small shake-up satellite peak for a few of the materials at 719 eV suggest that there is probably some oxidation of the material to γ-Fe_2O_3 during the exchange or purification process.[43]

Magnetic properties

Modification of the nanoparticle core by coating with organic films can have a significant effect on the nanoparticle's final magnetic moment.[44,45] Hence, vibrating sample magnetometry (VSM) was used to measure the magnetic properties both before and after exchange (Figure 4). The precursor, LA-stabi-
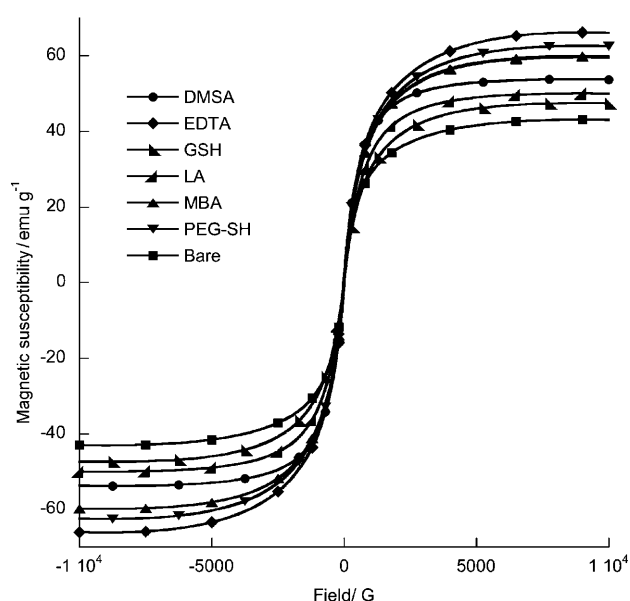
Figure 4. VSM magnetization curves of bare Fe_3O_4, Fe_3O_4-LA, and hydrophilic ligand-containing Fe_3O_4 nanoparticles.

lized Fe_3O_4, has a measured saturation magnetization value of 50 emu g^{-1} (Table 1). The MBA and GSH-stabilized Fe_3O_4 had a value only slightly less than the precursor material, confirming retention of magnetic character. However, the remainder of the stabilized nanoparticles showed an increase in magnetic moment following exchange. Since some of the materials obtained following the exchange process required a more intensive purification procedure, we attribute this occurrence to the further magnetic purification that accompanied the cleaning of the particles following exchange. The more rigorous cleaning removes some of the more soluble nanoparticles that do not settle quickly to the magnet and are thus removed from the measured sample. The more soluble, non-magnetic, or weakly ferrimagnetic particles, will be smaller and contribute a lower normalized magnetic moment to the overall sample mixture, hence their removal yields a sample with a higher overall magnetic moment on a per gram basis.

In addition to the relatively high magnetic moment for each of the nanoparticles, the VSM results also show that the particles are superparamagnetic, with no remnant coercivity. This is an important feature when using these materials as a sorbent since magnetic agglomeration of the particles prevents their dispersion in solution limiting their efficiency in metal ion uptake. Typically, iron oxide nanoparticles exhibit superparamagnetic behavior up to ca. 20 nm, thus the 8 nm size range of these materials ensures that the particles can be well-dispersed in solution but still have the benefit of the high surface area per mass. Although smaller iron oxide nanoparticles have a higher surface area per mass, they have a lower magnetic moment and can be more difficult to remove from solution. In contrast, commercially available, unfunctionalized iron oxide nanopowders that can be surface modified, tend to be polydisperse (hence include ferromagnetic particles > 20 nm that lead to magnetic agglomeration of the material) and the overall surface area per mass is drastically reduced.

Functionalized Fe_3O_4 as heavy metal sorbents

Determination of heavy metal uptake by functionalized Fe_3O_4 nanoparticle sorbents

For comparative and competitive evaluation, river water was spiked with seven different heavy metals to determine the effectiveness of each nanoparticle type as a heavy metal sorbent. The sorbent efficacy, described as the solid-phase distribution coefficient, or K_d, is a mass-weighted partition coefficient between the liquid supernatant phase and the solid sorbent phase according to the following equation:

$$K_d = \frac{(C_0 - C_f)}{C_f}\frac{V}{M} \tag{1}$$

in which, C_o and C_f are the initial and final concentrations of the target species in solution (measured by inductively coupled-mass spectrometry (ICP-MS)), V is the volume of solution in milliliters, and M is the sorbent mass in grams. The measured K_d values for each of the sorbents for each heavy metal are summarized in Table 2. The higher the K_d value, the more effective the sorbent material is at capturing and holding the target species. K_d is a direct measurement of sorbent affinity for an analyte under the conditions at which it is measured (which may impact the value). In general, K_d values of ca. 10^3 mL g^{-1} are considered good and those above

Table 2. K_d values of selected sorbents for heavy metal in river water.

Sorbent[a]				K_d			
---	Co	Cu	Ag	Cd	Hg	Pb	Tl
Activated carbon	790	26 000	27 000	1 300	31 000	190 000	21
Bare Fe_3O_4	1 600	7 400	13 000	2 400	16 000	78 000	4 000
Thiol resin	890	6 300	16 000	1 500	10 000	41 000	2 200
Fe_3O_4-MBA	20 000	440 000	27 000	20 000	7 800	1 800 000	6 400
Fe_3O_4-DMSA	3 200	91 000	110 000	7 400	390 000	280 000	13 000
Fe_3O_4-GSH	2 600	80 000	12 000	9 000	95 000	265 000	2 100
Fe_3O_4-PEG-SH	26 000	400 000	86 000	37 000	330 000	1 200 000	12 000
EDTA Resin	360 000	62 000	29 000	500 000	10 000	180 000	60
Fe_3O_4-EDTA	10 000	15 000	150 000	320	300 000	200 000	6 800

[a] Each magnetic nanoparticle sorbent was measured at 10^5 L/S (10^5 = 0.1 mg sorbent in 10 mL), and the commercial sorbents were measured at 10^4 L/S as the commercial sorbents did not have a measurable performance at the higher ratio. K_d values are for heavy metal extractions from filtered Columbia River water, pH 7.8. Activated carbon is Darco KB-B, thiol resin is GT-73, EDTA Resin is Chelex 100.

10^4 mL g^{-1} are outstanding. For trace level collection where sorbent performance is limited by chemical affinity, the K_d value provides a more meaningful value to describe sorbent performance than other parameters, such as a materials ion exchange capacity, which reflect performance under saturated conditions.

Comparative sorbent performance

For comparative performance studies, surface functionalized Fe_3O_4 nanoparticles were evaluated against select commercial sorbents of similar surface functionality as well as unfunctionalized iron oxide nanoparticles. River water spiked with heavy metals was selected as the matrix for evaluation since it provides a realistic environmental application challenge. It should be noted that the K_d values for the resin-based sorbents were measured at a liquid-to-solid (L/S) ratio of 10^4 (10^5 was the standard test conditions) since the resin particle precluded low masses (and higher L/S values) without substantial changes in comparative test conditions. The lower L/S ratio of the resins is unlikely to significantly affect the K_d values because the materials are not near saturation and the differences in the resin performance and the magnetic nanoparticle sorbent materials is large. Performance of the commercial resins will be comparatively discussed in conjunction with functionalized nanoparticles possessing similar surface chemistry.

Activated carbon (Darco KB-B) and unfunctionalized iron oxide nanoparticles (of similar core size to the functionalized nanoparticles) were also tested for comparison. Activated carbon and bare iron oxide nanoparticles both have very high surface areas (ca. 1600 m^2 g^{-1} for activated carbon[46] and ca. 124 m^2 g^{-1} for Fe_3O_4 nanoparticles) and are known to be chemically active surfaces for the absorption of a wide range of materials from solution. However, these materials do not have selective surface chemistry installed to increase affinity. Table 2 clearly shows that the surface functionalized sorbent

materials almost always have higher K_d values (depending upon surface chemistry and analyte). The bare iron oxide nanoparticles usually had a much lower affinity for the metals when compared to the functionalized sorbents demonstrating the essential value of surface functionalization to increase and tune the chemical activity of the magnetic nanoparticle sorbent material.

As explained by Pearson's hard–soft acid–base theory (HSAB),[47] thiol functionalized materials should have a high affinity for softer metals; in Table 2 sorbents functionalized with thiol surface chemistries can be observed to have the highest affinities for the softer analytes (Cu, Ag, Hg, and Pb). GT-73 is a commonly used thiol-containing commercial resin for the adsorption of heavy metals. When metal uptake with GT-73 is compared to the thiol containing ligand-stabilized nanoparticles (PEG-SH, DMSA, GSH, and MBA) the K_d values for the functionalized nanoparticles far exceed the K_d for the resin in almost all cases. The specific order of selectivity for the full range of thiol sorbents is shown in Scheme 1. The DMSA functionalized nanoparticles show excellent affinity for the softer heavy metals such as Hg and Ag, whereas the nanoparticles functionalized with PEG-SH and MBA show a superior affinity for Pb, Cu, and Hg (PEG-SH only). The free thiol-containing MBA and PEG-SH would be expected to have much higher affinity for Hg than Pb, but experimentally show higher affinity for Pb. We believe this is attributed to the formation of disulfide bonds in the free ligand prior to attachment to the nanoparticle yielding a carboxylic acid rather than a thiol-binding moiety on the periphery of the nanoparticle ligand shell. This explanation is further corroborated by the excessive amount of ligand observed on the MBA particles by TGA, and the two-staged mass loss suggesting the loss of both the mono-thiol and disulfide containing ligands. The PEG-SH nanoparticles show a very high affinity for Pb but still have an excellent K_d for Hg as well, possibly suggesting the presence of a mix of thiol and disulfide ligands. Additionally, the GSH-modified nanoparticles containing both carboxylate and thiol binding moieties show a greater affinity for Pb, followed by Hg and Cu.

EDTA is a well-known heavy metal chelating ligand with a high affinity for multivalent metals. We evaluated EDTA-modified Fe_3O_4 nanoparticles and Chelex 100, a commonly used EDTA-containing polymeric resin material. Heavy metal K_d values for the two EDTA-based materials are shown in the lower portion of Table 2. Both EDTA-based sorbent materials have good K_d values, typically above 10^4 for most heavy metals. For all the sorbents measured, Chelex 100 has the best affinity measured for Cd and Co and the EDTA Fe_3O_4 nanoparticles have the best K_d value for Hg, Pb, and Ag. Closer examination of the data in Table 2 shows that the Chelex 100 resin has higher K_d values for harder analytes and the EDTA functionalized Fe_3O_4 has better K_d values for softer analytes. The order of selectivity for Chelex 100 is Cd, Co, Pb, Cu, Ag, Hg ≫ Tl and for the EDTA Fe_3O_4 nanoparticles the order of selectivity is significantly different: Hg, Pb, Ag > Cu, Co, Tl > Cd. Why the relative selectivity of the EDTA ligand changes relative to the commercial sorbent selectivity is a matter of supposition based on the available data, but binding affinity and selectivity are strongly

↖↖ These are not the final page numbers!

impacted by hard–soft interactions, analyte speciation, and analyte valency. The EDTA ligand is bound to the resin substrate differently than it is to the nanoparticles. The EDTA ligands in Chelex 100 resin are bound through the terminal N leaving the ligand to function as expected with carboxylic acid terminated arms free to form the chelation cage (more similarly to its behavior in solution). In the nanoparticles, a portion of the carboxylic acids of the EDTA ligands are bound to the surface, likely exposing more of the amine to the metal ion during complexation, possibly resulting in enhanced selectivity for the softer transition metals and reduced affinity for the harder metal species.

Whereas the selectivity of the magnetic nanoparticle sorbents depends upon the ligand, the K_d data clearly shows they can be made to have excellent affinity for heavy metals, typically better than commercial sorbent materials. In addition to high affinities making the magnetic nanoparticle sorbents effective for sorption of trace level analytes from solution, they also have the benefit of simple removal from the analyte-containing solution. The commercial resins must be centrifuged or filtered from the treated matrix for analysis, whereas the solutions containing the magnetic sorbents can simply be placed on a magnet for fast removal of the analyte-bound sorbent.

Conclusions

We have described the functionalization of superparamagnetic iron oxide nanoparticles using a straightforward precursor synthesis followed by a facile ligand exchange process to bind readily available affinity ligands onto the nanoparticle surface. This technique allows for tailoring of the surface chemistry to impart the specificity and affinity toward the target analytes (heavy metals of environmental concern). The resultant functionalized magnetic Fe_3O_4 nanoparticles are easy to synthesize and are excellent sorbents for a variety of heavy metal contaminants depending on the surface ligand installed. The described functionalized nanoparticles typically have analyte affinities much higher than commercial sorbent materials, and in addition, have the benefit of simple, rapid magnetic removal from the analyte containing solution, avoiding the issues with centrifugation and filtration. Further, the ability to magnetically manipulate the sorbent materials opens up a wide range of applications that would involve trapping the nanoparticles to form a sorbent bed or column and removing the contaminants under flow conditions across the trapped nanoparticles. This will allow these materials to be used in relatively large-scale water remediation efforts where batch contact is impractical.[18]

Thiol and EDTA surface chemistries have been installed on the Fe_3O_4 nanoparticles and were shown to be highly effective, magnetically active sorbent materials. The reported synthetic method could be used to install additional relevant surface chemistries chosen to target other biological and chemical analytes, for example, semipolar organics, radionuclides, proteins, and nucleic acids, of importance to environmental monitoring, decontamination, and remediation. Extending the versatility of the materials even further, the thiol, EDTA, and other primary ligands could be used in subsequent reactions as a base layer

upon which more complex molecular structures could be built off on the nanoparticle surface using standard organic chemistry linkage methods such as click chemistry and amide coupling reactions. In addition, these materials could play a vital role in the development of novel environmentally benign ("green") materials for environmental sensing and remediation.[49, 50] In summary, we have shown a simple, flexible method for the preparation of highly effective, superparamagnetic nanoparticle sorbent materials and demonstrated their efficacy for the capture of toxic heavy metals from aquatic systems of relevance to the global problem of drinking water decontamination.

Experimental Section

General considerations

The α-thio-ω-(propionic acid) hepta(ethylene glycol) (PEG-SH) ligand was purchased from Iris Biotech (Marktredwitz, Germany). 4-mercaptobutyric acid (MBA) was purchased from Pfaltz and Bauer (Waterbury, CT). L-glutathione, reduced (GSH), ethylenediamine tetraacetic acid disodium salt dihydrate (EDTA), *meso*-2,3-dimercaptosuccinic acid (DMSA), and lauric acid (LA) ligands, as well as all of the reagents for the preparation for the LA-stabilized Fe_3O_4 were purchased from Aldrich and used as received. Darco KB-B activated charcoal was purchased from Aldrich, GT-73 thiol resin was purchased from Rohm and Haas (Philadelphia, PA), and Chelex 100 EDTA resin was purchased from BioRad (Hercules, CA). All water used in the purification of the materials was 18 MΩ-cm. River water used in extractions was collected from the Columbia River, Richland, WA, and filtered through a 0.45 μ cellulose membrane (MF-Millipore). LA-stabilized nanoparticles were first prepared for use as the organic soluble precursor nanoparticle in ligand exchange reactions. Ligand exchange reactions were carried out in glass scintillation vials (20 mL).

Synthesis of Fe_3O_4-LA precursor nanoparticle

The nanoparticles were synthesized according to the method described by Sun et al,[20] with some modifications (see the Supporting Information). The resultant nanoparticles were easily dispersed in hexanes and toluene and showed an average core diameter of 8.3 ± 2 nm by TEM.

Synthesis of water-soluble ligand-stabilized nanoparticles by ligand exchange

Fe_3O_4-LA (10 mg mL^{-1}) suspended in toluene (2 mL) was combined with the desired ligand (15 mg mL^{-1}) dissolved in methanol (2 mL) in a vial. The mixture was stirred overnight (18 h to 24 h) at 1100 rpm at RT. The nanoparticles were then washed several times with ethanol, acetone, and water with magnetic decantation to remove excess ligand and species with mixed-ligand shells. The collected water-soluble ligand-stabilized Fe_3O_4 was dried under argon.

Nanoparticle characterization

An Autosorb-6B (Quantachrome Corp., FL) surface area analyzer was used to determine the BET surface area of the synthesized materials by nitrogen adsorption at 77 K.

These are not the final page numbers! ↗↗

FTIR spectra were obtained by collecting 100 scans at 4 cm^{-1} resolution in the wavelength range of 450–4000 cm^{-1} on a Nicolet Magna-IR 760 spectrometer (Thermo Nicolet, WI). Sample windows were obtained by pressing a small amount of nanoparticles into a KBr pellet.

Magnetometry of the iron oxide nanoparticles was performed using a Lakeshore 7404 VSM at RT using quartz sample ampoules. Details of the measurement and the instrument parameters are given in the Supporting Information.

TEM images of the nanoparticles were obtained using a JEOL 2010 TEM with an acceleration voltage of 200 kV. Nanoparticles were suspended in ethanol and sprayed onto carbon and Formvar coated copper grids in preparation for imaging. Size analysis of the nanoparticles was performed with a public domain image analysis program using a method described previously.[48]

Determination of ligand density on the iron oxide core was calculated using TGA. TGA for all samples was run on a Netzsch Simultaneous Thermal Analyzer 409 C/CD (Netzsch Instruments Inc, Burlington, MA) with a heat ramp rate of 10 °C min^{-1} from 40 to 850 °C under He flow (10 mL min^{-1}). Data was worked up using Netzsch Proteus software for thermal analysis.

XPS measurements were performed using a Physical Electronics Quantum 2000 scanning ESCA microprobe. Details of the measurements and the instrumental parameters are given in the Supporting Information.

Extraction of heavy metals using functionalized magnetic nanoparticle sorbents

The filtered river water samples were spiked with metal ions to obtain 0.5 ppm (each) of Co, Cu, Ag, Cd, Hg, Tl, and Pb. The prepared metal solution (10 mL) was aliquoted into a polypropylene tube (15 mL) and spiked with a small volume of nanoparticles suspended in deionized water to obtain a liquid-to-solid ratio of 10^5 (L/S, expressed as mL g^{-1} hereafter). The samples were agitated for 2 h at 160 rpm on an orbital shaker. After 2 h the nanoparticles were separated from the solution using a 1.2 T Neodymium Iron Boron (NdFeB) magnet, usually requiring approximately 10 seconds. After another 30 seconds on the magnet to ensure complete nanoparticle removal from solution, the supernatant was removed and stored in 1% HNO$_3$ prior to analysis. All of the metal extraction experiments were performed in duplicate and averaged K_d values were reported with standard deviations that were typically less than 10%. Error values for large K_d values may be higher owing to the small amount of analyte left to measure in contact solutions.

ICP-MS analysis of metal solutions

Heavy metal spiked river water samples were analyzed following nanoparticle sorption experiments using ICP-MS (Agilent 7500 ce, Agilent Technologies, CA). Calibration curves of metal ions were constructed from 0, 0.1, 0.5, 10, 50, and 100 ppb of each metal ion in 1 vol.% concentrated HNO$_3$ in deionized water ($R^2 > 0.9995$). Ge, Y, and In were used as internal standards for metals of similar mass at 10 ppb (Ge for Co, Cu, Fe; Y for Cd and Ag; Ir for Pb, Hg, and Tl). The lowest metal concentration in the samples to be measured was at least 3-fold larger than the experimental detection limit of the instrument. All solution assays were run in triplicate.

[1] http://www.epa.gov/OGWDW/hfacts.html (last accessed March 18, **2010**).

[2] G. E. Fryxell, in *Environmental Applications of Nanomaterials* (Eds.: G. E. Fryxell, G. Cao), Imperial College Press, London, **2007**, pp. 159–178.

[3] W. Yantasee, C. L. Warner, T. Sangvanich, R. S. Addleman, T. G. Carter, R. J. Wiacek, G. E. Fryxell, C. Timchalk, M. G. Warner, *Environ. Sci. Technol.* **2007**, *41*, 5114–5119.

[4] W. Yantasee, K. Hongsirikarn, C. L. Warner, D. Choi, T. Sangvanich, M. B. Toloczko, M. G. Warner, G. E. Fryxell, R. S. Addleman, C. Timchalk, *Analyst* **2008**, *133*, 348–355.

[5] M. G. Warner, C. L. Warner, R. S. Addleman, W. Yantasee, in *Magnetic Nanomaterials* (Ed.: C. Kumar), Vol. 4, Wiley-VCH, Weinheim, **2009**, pp. 311–344.

[6] S. S. Banerjee, D.-H. Chen, *J. Hazard. Mater.* **2007**, *147*, 792–799.

[7] Y.-C. Chang, S.-W. Chang, D.-H. Chen, *React. Funct. Polym.* **2006**, *66*, 335–341.

[8] Y.-C. Chang, D.-H. Chen, *J. Colloid Interface Sci.* **2005**, *283*, 446–451.

[9] N. Joumaa, P. Toussay, M. Lansalot, A. Elaissari, *J. Polym. Sci., Part A: Polym. Chem.* **2008**, *46*, 327–340.

[10] A.-F. Ngomsik, A. Bee, J.- M. Siaugue, V. Cabuil, G. Cote, *Water Res.* **2006**, *40*, 1848–1856.

[11] S. Shin, J. Jang, *Chem. Commun.* **2007**, 4230–4232.

[12] B. Hai, J. Wu, X. Chen, J. D. Protasiewicz, D. A. Scherson, *Langmuir* **2005**, *21*, 3104–3105.

[13] F. M. Koehler, M. Rossier, M. Waelle, E. K. Athanassiou, L. K. Limbach, R. N. Grass, D. Gunther, W. J. Stark, *Chem. Commun.* **2009**, 4862–4864.

[14] L. L. Vatta, J. Kramer, K. R. Koch, *Sep. Sci. Technol.* **2007**, *42*, 1985–2002.

[15] J. Hu, G. Chen, I. M. C. Lo, *Water Res.* **2005**, *39*, 4528–4536.

[16] J. Hu, G. Chen, I. M. C. Lo, *J. Environ. Eng. Div. (Am. Soc. Civ. Eng.)* **2006**, *132*, 709–715.

[17] J. Hu, I. M. C. Lo, G. Chen, *Sep. Purif. Technol.* **2007**, *56*, 249–256.

[18] C. T. Yavuz, J. T. Mayo, W. W. Yu, A. Prakash, J. C. Falkner, S. Yean, L. Cong, H. J. Shipley, A. Kan, M. Tomson, D. Natelson, V. L. Colvin, *Science* **2006**, *314*, 964–967.

[19] S.-H. Huang, D.-H. Chen, *J. Hazard. Mater.* **2009**, *163*, 174–179.

[20] S. Sun, H. Zeng, D. B. Robinson, S. Raoux, P. M. Rice, S. X. Wang, G. Li, *J. Am. Chem. Soc.* **2004**, *126*, 273–279.

[21] R. De Palma, S. Peeters, M. J. Van Bael, H. Van den Rul, K. Bonroy, W. Laureyn, J. Mullens, G. Borghs, G. Maes, *Chem. Mater.* **2007**, *19*, 1821–1831.

[22] N. Kohler, G. E. Fryxell, M. Zhang, *J. Am. Chem. Soc.* **2004**, *126*, 7206–7211.

[23] M. Kim, Y. Chen, Y. Liu, X. Peng, *Adv. Mater.* **2005**, *17*, 1429–1432.

[24] S. Mohapatra, S. K. Mallick, T. K. Maiti, S. K. Ghosh, P. Pramanik, *Nanotechnology* **2007**, *18*, 385102.

[25] C. Yee, G. Kataby, A. Ulman, T. Prozorov, H. White, A. King, M. Rafailovich, J. Sokolov, A. Gedanken, *Langmuir* **1999**, *15*, 7111–7115.

[26] W. H. Binder, H. Weinstabl, R. Sachsenhofer, *J. Nanomater.* **2008**, article ID 383020..

[27] A. K. Boal, K. Das, M. Gray, V. M. Rotello, *Chem. Mater.* **2002**, *14*, 2628–2636.

[28] A. B. Bourlinos, A. Bakandritsos, V. Georgakilas, D. Petridis, *Chem. Mater.* **2002**, *14*, 3226–3228.

[29] M. G. Warner, S. M. Reed, J. E. Hutchison, *Chem. Mater.* **2000**, *12*, 3316–3320.

[30] Y.-M. Huh, Y.-W. Jun, H.-T. Song, S. Kim, J.-S. Choi, J.-H. Lee, S. Yoon, K.-S. Kim, J.-S. Shin, J.-S. Suh, J. Cheon, *J. Am. Chem. Soc.* **2005**, *127*, 12387–12391.

[31] G. E. Fryxell, S. V. Mattigod, Y. Lin, H. Wu, S. Fiskum, K. Parker, F. Zheng, W. Yantasee, T. S. Zemanian, R. S. Addleman, J. Liu, K. Kemner, S. Kelly, X. Feng, *J. Mater. Chem.* **2007**, *17*, 2863–2874.

[32] R. S. Tejowulan, W. H. Hendershot, *Environ. Pollut.* **1998**, *103*, 135–142.

[33] L. Di Palma, P. Ferrantelli, C. Merli, F. Biancifiori, *J. Hazard. Mater.* **2003**, *103*, 153–168.

[34] A. H. Lu, E. L. Salabas, F. Schueth, *Angew. Chem.* **2007**, *119*, 1242–1266; *Angew. Chem. Int. Ed.* **2007**, *46*, 1222–1244.

[35] T. K. Jain, M. A. Morales, S. K. Sahoo, D. L. Leslie-Pelecky, V. Labhasetwar, *Mol. Pharm.* **2005**, *2*, 194–205.

[36] L. Shen, P. E. Laibinis, T. A. Hatton, *Langmuir* **1999**, *15*, 447–453.

[37] M. De Cuyper, M. Joniau, *Langmuir* **1991**, *7*, 647–652.

[38] Y. Sahoo, H. Pizem, T. Fried, D. Golodnitsky, L. Burstein, C. N. Sukenik, G. Markovich, *Langmuir* **2001**, *17*, 7907–7911.

[39] R. M. Silverstein, G. C. Bassler, T. C. Morrill, *Spectrometric Identification of Organic Compounds*, 5th ed., John Wiley and Sons, New York, **1991**.

[40] J. F. Moulder, W. F. Stickle, P. E. Sobel, K. D. Bomben, *Handbook of X-Ray Photoelctron Spectroscopy*, Physical Electronics, **1995**.

[41] Q. Liu, Z. Xu, *Langmuir* **1995**, *11*, 4617–4622.

[42] M. Volmer-Uebing, M. Stratmann, *Appl. Surf. Sci.* **1992**, *55*, 19–35.

[43] Y. Gao, S. A. Chambers, *J. Cryst. Growth* **1997**, *174*, 446–454.

[44] T. J. Daou, J. M. Grenech, G. Pourroy, S. Buathong, A. Derory, C. Ulhaq-Bouillet, B. Donnio, D. Guillon, S. Begin-Colin, *Chem. Mater.* **2008**, *20*, 5869–5875.

[45] D. A. van Leeuwen, J. M. van Ruitenbeek, L. J. de Jongh, A. Ceriotti, G. Pacchioni, O. D. Heberlen, N. Rausch, *Phys. Rev. Lett.* **1994**, *73*, 1432–1435.

[46] http://www.sigmaaldrich.com (last accessed March 18, **2010**).

[47] R. G. Pearson, *J. Am. Chem. Soc.* **1963**, *85*, 3533–3539.

[48] G. H. Woehrle, J. E. Hutchison, S. Özkâr, R. G. Finke, *Turk. J. Chem.* **2006**, *30*, 1–13.

[49] M. G. Warner, G. L. Succaw, J. E. Hutchison, *Green Chem.* **2001**, *3*, 267–270.

[50] T. Masciangioli, W. Zhang, *Environ. Sci. Technol.* **2003**, *37*, 102 A-108 A.

FULL PAPERS

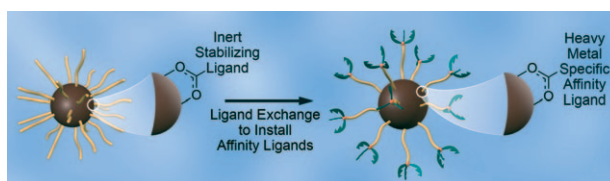*C. L. Warner, R. S. Addleman, A. D. Cinson,*
T. C. Droubay, M. H. Engelhard,
M. A. Nash, W. Yantasee, M. G. Warner*

■■ – ■■

High-Performance,
Superparamagnetic, Nanoparticle-
Based Heavy Metal Sorbents for
Removal of Contaminants from
Natural Waters

Superparamagnetic iron man: The synthesis and characterization of superparamagnetic, iron oxide nanoparticle-based heavy metal sorbents with various surface chemistries, which demonstrate excellent affinity for the separation of heavy metals in contaminated natural water systems is described. Our method has the unique advantage that the analyte reactivity is incorporated into the nanoparticle ligand shell without altering the desirable properties of the starting nanoparticle.

↖↖ These are not the final page numbers!